Quantum Chemical Investigation of the Electronic Spectra of the Keto, Enol, and Keto−Imine Tautomers of Cytosine

Katarina Tomić, Jörg Tatchen, and Christel M. Marian*

Institute of Theoretical and Computational Chemistry, Heinrich-Heine-University, Universitätsstrasse 1, D-40225 Düsseldorf, Germany

Received: March 23, 2005; In Final Form: July 20, 2005

The low-lying excited singlet states of the keto, enol, and keto−imine tautomers of cytosine have been investigated employing a combined density functional/multireference configuration interaction (DFT/MRCI) method. Unconstrained geometry optimizations have yielded out-of-plain distorted structures of the $\pi \rightarrow \pi^*$ and $n \rightarrow \pi^*$ excited states of all cytosine forms. For the keto tautomer, the DFT/MRCI adiabatic excitation energy of the $\pi \rightarrow \pi^*$ state (4.06 eV including zero-point vibrational energy corrections) supports the resonant two-photon ionization (R2PI) spectrum (Nir et al. *Phys. Chem. Chem. Phys.* **2002**, *5*, 4780). On its S_1 potential energy surface, a conical intersection between the $^1\pi\pi^*$ state and the electronic ground state has been identified. The barrier height of the reaction along a constrained minimum energy path amounts to merely 0.2 eV above the origin and explains the break-off of the R2PI spectrum. The $^1\pi\pi^*$ minimum of the enol tautomer is found at considerably higher excitation energies (4.50 eV). Because of significant geometry shifts with respect to the ground state, long vibrational progressions are expected, in accord with experimental observations. For the keto−imine tautomer, a crossing of the $^1\pi\pi^*$ potential energy surface with the ground-state surface has been found, too. Its $n \rightarrow \pi^*$ minimum (3.27 eV) is located well below the conical intersection between the $\pi \rightarrow \pi^*$ and S_0 states, but it will be difficult to observe because of its small transition moment. The identified conical intersections of the $\pi \rightarrow \pi^*$ excited states of the keto cytosine tautomers are made responsible for the ultrafast decay to the electronic ground states and thus may explain their subpicoseconds lifetimes.

1. Introduction

The nucleobases represent one of the main building blocks of life. Because of their great biological importance, they have been the subject of numerous theoretical and experimental investigations that were reviewed recently by Crespo-Hernández et al.[1] Detailed knowledge of their electronic structure and spectral properties is indispensable for a complete understanding of the biological functionality of polynucleosides, in particular with respect to photostability.

Solution spectra of cytosine are broad and structureless.[2,3] It is therefore very difficult to extract information about the electronic and nuclear structure of electronically excited cytosine from these spectra. Time-resolved transient absorption[4,5] or fluorescence up-conversion[6] spectra in aqueous solution yield decay rates that are best fitted by biexponential functions with a femtosecond component and a picosecond component. The origin of the biexponential decay is not clear. It might be a tautomer effect (as assumed for adenine), might involve two electronically excited states of the same tautomer, or may even be caused by a rapid change of electronic transition moments with nuclear geometry relaxation in the electronically excited state.

Fundamental insight is gained from the examination of the excited states of the free molecule in the gas phase. Here the pyrimidine nucleobase cytosine appears in three different tautomeric forms: the keto, enol, and keto−imine forms, which are represented in Figure 1. Differences in the electronic structures of the tautomers produce differences in their spectra.

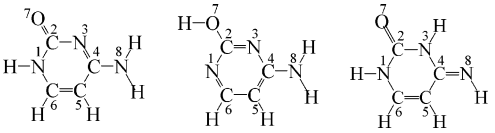

Figure 1. Tautomeric forms of cytosine: keto (left), enol (middle), keto−imine (right). The numbering of the centers agrees with the conventions for pyrimidine.

High-resolution resonant two-photon ionization (R2PI) spectra of cytosine were recorded close to the band origins of the lowest-lying transitions.[7] The experimentally observed gas-phase vibronic spectrum of cytosine[8] is divided in two spectral regions which are separated by about 4000 cm^{-1}. The spectrum around 32 000 cm^{-1} has been assigned to the keto tautomer and the spectrum around 36 000 cm^{-1} to the enol tautomer. Femtosecond transient ionization signals of electronically excited cytosine prepared at 267 nm ($\approx$37 450 cm^{-1}) in a molecular beam show a biexponential decay of the excited-state population.[9] The tautomer(s) responsible for this behavior have not been identified so far. In a molecular beam microwave spectroscopy study[10] the population of the keto−imine tautomer is estimated to be only one-quarter of the population of the other tautomers. Its electronic excitation spectrum has not been observed in experiment.

Previous theoretical work by Sobolewski and Domcke on the guanine−cytosine (GC) base pair[11] opened the question whether the geometry of photoexcited cytosine is planar or nonplanar. In this paper, two fast relaxation pathways of the electronically excited base pair to the electronic ground state are described.

* Corresponding author. E-mail: Christel.Marian@uni-duesseldorf.de. URL: http://www.theochem.uni-duesseldorf.de

10.1021/jp051510o CCC: $30.25
Published on Web 08/30/2005

The mechanism dubbed SPT involves an electron transfer from guanine to cytosine followed by a single proton transfer. The second pathway named ETH proceeds on a potential energy hypersurface corresponding to a locally excited electronic structure of cytosine. Here, an intersection between the S_1 and S_0 potential energy hypersurfaces of the base pair takes place at moderate energies for a structure in which the $C_5{=}C_6$ bond (see Figure 1) of the cytosine ring is twisted. The rapid decay of the excited-state population via these pathways is believed to be responsible for the ultrashort lifetime of the Watson−Crick base pair observed in experiment.[12] The detection of the ETH pathway[11] led us to the question whether a similar conical intersection can be found in the bare cytosine. Merchán and Serrano-Andrés[13] observed a different conical intersection between the $\pi\pi^*$ state and the ground state of the bare keto−cytosine. In the latter case, the decisive coordinate appears to be the CO bond stretch.

Guided by these findings, we study here the behavior of the photoexcited cytosine tautomers. The main aim of our study is to compute the vertical and adiabatic electronic excitation spectra of the above-mentioned tautomers and to compare the results with the experimental ones. To this end, we have calculated geometries and relative energies of the ground and low-lying excited states as well as normal modes in the ground states.

2. Methods and Technical Details

All calculations have been performed employing the valence triple-ζ basis set with polarization functions (d,p) from the TURBOMOLE library.[14] This basis set is denoted by TZVP in the following.

The procedure that we have used to obtain geometries and relative energies has been recently applied to the investigation of adenine by Marian.[15] Full geometry optimizations have been carried out utilizing the TURBOMOLE program package, version 5.6.[16,17] Optimizations of the ground and excited states have been performed at the level of density functional theory (DFT) and time dependent density functional theory (TDDFT), respectively. To check the results with respect to the influence of different density functionals, calculations of the vertical electronic spectra have been performed employing the equilibrium nuclear arrangements obtained for both the BH-LYP and the B3-LYP hybrid functionals.[18,19] For the calculation of the adiabatic spectra, the BH-LYP optimized geometries were employed. Constrained minimum energy paths (CMEP) were obtained from partial optimizations in internal coordinates, employing the EF.X program.[20]

We have used the SNF program[21] to calculate normal modes in the ground states of the tautomers. The vibrational frequencies have been computed at the B3-LYP geometry and have been scaled by a common factor of 0.9614.[22]

For the determination of the singlet electronic states of cytosine, we applied the combined density functional theory/multireference configuration interaction (DFT/MRCI) method by Grimme and Waletzke.[23] This semiempirical method was shown to yield excellent electronic spectra of organic molecules at reasonable computational cost. Using an effective, parametrized Hamiltonian, the DFT/MRCI includes both dynamic (DFT) and static (MRCI) electron correlation. The problem of double counting of electron correlation is avoided mostly by introducing an exponential damping factor into the Hamiltonian. The configuration state functions (CSFs) in the MRCI expansion are built up from Kohn−Sham (KS) orbitals. Optimized parameter sets for the effective DFT/MRCI Hamiltonian are available in combination with the BH-LYP functional. The initial set of CSFs can be generated automatically in a complete active space type procedure and is then iteratively improved. The MRCI expansion is kept moderate by extensive configuration selection. The DFT/MRCI approach gives relative energies of high quality, with a root-mean-square deviation from experimental reference data by about 0.15 eV.[23] Beside an excellent description of the energy, the DFT/MRCI provides a reliable prediction of properties. More details about the method can be found in the original publication by Grimme and Waletzke.[23]

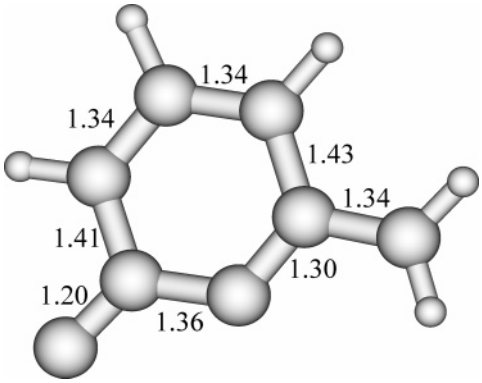

Figure 2. Ground-state geometry of the keto tautomer optimized with the BH-LYP functional. DFT/MRCI energy: $-394.847853E_H$. Dipole moment at the DFT/MRCI level: 6.82 D.

Molecular KS orbitals, optimized for the dominant closed shell determinant of the electronic ground state, were employed as a one-particle basis for the MRCI runs. In the latter step, all valence electrons were correlated. For planar nuclear arrangements, eigenvalues and eigenvectors of four singlet states were determined in each irreducible representation (A′, A″). At lower symmetry points, the eight lowest singlet states were determined.

The DFT/MRCI adiabatic excitation energies are improved by taking into account zero-point vibrational energy (ZPVE) corrections. These are obtained by performing a normal-mode analysis in both ground and excited states. The zero-point energies are scaled with a common factor for the BH-LYP functional of 0.9257. The scaling factor is estimated on the basis of a DFT study of vibrational spectra,[24] in which observed and calculated fundamental vibrational frequencies at the BH-LYP level are compared for a set of molecules.

3. Results and Discussion

Cartesian coordinates of ground and excited-state minima of all tautomers can be found in the Supporting Information. This data collection also includes the coordinates of nuclear structures at or close to conical intersections between the ground state and the first excited singlet $\pi \rightarrow \pi^*$ states of the keto and the keto−imine tautomers.

3.1. Keto Tautomer of Cytosine. We begin the investigation of the keto tautomer with the ground-state geometry optimization. The DFT/MRCI energy, geometry parameters optimized at the BH-LYP level of theory, and the dipole moment of the ground state of keto cytosine are presented in Figure 2. As a general trend, the B3-LYP functional gives somewhat larger bond distances (1 pm). In the nuclear arrangement optimized with the BH-LYP functional all nuclei lie in a common plain. The B3-LYP minimum structure shows slight out-of-plane distortions which include amino group pyramidalization, but the energy difference between the C_1-symmetric minimum and the C_s-symmetric saddle-point amounts to merely 1 cm^{-1} at this level of theory. From the calculated vibrational frequency of the pyramidalization mode (166 cm^{-1}), we conclude that the

TABLE 1: Harmonic Vibrational Frequencies [cm^{-1}] for the NH Stretching Modes in the Ground State of the Keto Cytosine[a]

	DFT(B3-LYP, scaled)	experiment[25]	experiment[26]
NH_2(s)	3461	3450	3452
N_1H	3474	3475	3472
NH_2(a)	3590	3575	3573

[a] Key: (s) symmetric vibrations; (a) antisymmetric vibrations.

TABLE 2: Vertical Singlet Excitation Energies ΔE [eV] (DFT/MRCI, TZVP Basis, BH-LYP Geometry) and Dipole Transition Oscillator Strengths $f(r)$ of Keto Cytosine

		DFT/MRCI, present work		
state		ΔE	$f(r)$	dominant excitation(s)
S_1	$2^1A'$	4.83	0.0803	$\pi_H \rightarrow \pi^*_L$
S_2	$1^1A''$	5.02	0.0022	$n_O \rightarrow \pi^*_L$
S_3	$2^1A''$	5.50	0.0014	$n_N \rightarrow \pi^*_L$
S_4	$3^1A'$	5.67	0.1807	$\pi_{H-1} \rightarrow \pi^*_L$
S_5	$3^1A''$	5.91	0.0000	$n_O \rightarrow \pi^*_{L+1}$, $n_N \rightarrow \pi^*_{L+1}$
S_6	$4^1A''$	6.32	0.0008	($\pi_H \rightarrow$ Ryd)[a]
S_7	$4^1A'$	6.60	0.6938	$\pi_H \rightarrow \pi^*_{L+3}$

[a] When diffuse functions are added to the basis, the energy of the Rydberg excitations is expected to decrease considerably.

first vibrational level ($v = 0$) should be located well above the barrier to planarity. Therefore, we have computed the vertical excitation spectrum in C_s symmetry.

According to our investigations the keto form is the second most stable tautomer in the gas phase. The dipole moment of this form of cytosine is the largest one among the three tautomers. It will, therefore, be preferentially stabilized in polar solvents. The scaled frequencies of the NH stretching modes in the ground state are given in Table 1. They compare favorably with the values measured in IR−UV double resonance experiments[25] and IR spectra recorded in liquid helium nanodroplets.[26]

3.1.1. The Vertical Absorption Spectrum. To describe the electronic structure of the excited states, it is necessary to characterize the frontier molecular orbitals. The highest occupied molecular orbital (HOMO) is a π-type orbital with large amplitude at the oxygen site and in the following we denote it by π_H. The second highest occupied molecular orbital (HOMO-1) is also of π-type and we designate as π_{H-1}. The third highest occupied molecular orbital (HOMO-2) is an n-type orbital with large amplitude for the oxygen lone-pair orbital, denominated by n_O in the following. The fourth highest occupied molecular orbital is also of n-type, but the amplitude is concentrated on the nitrogen (N_3) lone-pair orbital and we designate it as n_N. Concerning the virtual orbitals, the lowest-lying unoccupied molecular orbital (LUMO) is a π-type orbital, designated by π^*_L. It is delocalized over the whole molecule. Using the same notation for the higher valence molecular orbitals, we denote them by π^*_{L+1}, π^*_{L+2}, etc.

The vertical electronic spectrum at the minimum of the ground-state potential energy surface of the keto tautomer was computed using C_s point group symmetry. The relative DFT/MRCI excitation energies, oscillator strengths and dominant excitations are shown in Table 2. The lowest-lying excited state corresponds to the HOMO−LUMO transition. The transition is accompanied by a charge transfer from the oxygen into the ring and has a medium oscillator strength. The second excited singlet state is an $n \rightarrow \pi^*$ state and arises from the excitation of the n_O to the π^*_L orbital. This transition is weak, which is expected for $n \rightarrow \pi^*$ singlet excitations of heteroaromatic compounds. The third singlet state (S_3) results from $n_N \rightarrow \pi^*_L$ excitation and is found to have a small oscillator strength, too. S_4 arises from a $\pi_{H-1} \rightarrow \pi^*_L$ excitation. It is accompanied by a charge transfer from the NH_2 group into the ring and appears as very strong transition.

When we compare the vertical spectra obtained at the B3-LYP and BH-LYP geometries, we conclude that there is no difference in the ordering of the low-lying excited states with respect to different functionals used in the optimizations. Nevertheless, we notice that the B3-LYP geometry exhibits lower excitation energies. The energy of the lowest $\pi \rightarrow \pi^*$ state changes from 4.83 eV at the BH-LYP geometry to 4.68 eV at the B3-LYP geometry. At the BH-LYP geometry the lowest $n \rightarrow \pi^*$ state has the energy of 5.02 eV, while at the B3-LYP geometry its energy is 4.90 eV. These findings are a consequence of the elongated bond lengths of the B3-LYP equilibrium geometry with respect to the BH-LYP optimized nuclear arrangement. They are therefore expected as a general trend.

Here we compare our results with previous theoretical treatments of the vertical spectrum of cytosine. For the comparison, we use only a few low-lying excited states. In the higher-energy region valence states mix with the Rydberg states and to describe such states it would be necessary to use extended basis sets. We find good agreement with the results of Petke et al.[27] obtained by extended-basis RPA calculations. They find that the lowest-lying $^1\pi\pi^*$ state appears at 4.61 eV. This value shows better agreement with the DFT/MRCI energy at the B3-LYP geometry (4.68 eV) than with the one at the BH-LYP geometry (4.83 eV). They also predict that the two next states of $n \rightarrow \pi^*$ character appear at 4.95 and 5.43 eV, respectively. This is in accordance with our findings for the two $n \rightarrow \pi^*$ states computed at the BH-LYP geometry (Table 2). Fülscher and Roos[28] calculated CASPT2 excitation energies of keto cytosine. They found the lowest $\pi \rightarrow \pi^*$ excited state to occur at 4.39 eV. This value is much lower than ours. The first excited singlet $n \rightarrow \pi^*$ state is computed by CASPT2 to appear at 5.00 eV. This value agrees with the energy of 5.02 eV that we have computed for the $^1n\pi^*$ state. Nevertheless, the first state arises from an excitation of a nitrogen lone-pair electron (n_N) in their CASPT2 study, while we find it to originate from an excitation of an oxygen lone-pair electron (n_O). Our finding is supported by many other theoretical investigations.[13,29] In another CASPT2 study by Merchán and Serrano-Andrés,[13] the lowest-lying $n \rightarrow \pi^*$ state appears to be the $n_O\pi^*$ state with an excitation energy of 4.88 eV, which is in accord with our result. The energies of the $\pi \rightarrow \pi^*$ state (4.64 eV) and the $n \rightarrow \pi^*$ state (4.77 eV) obtained by Shukla and Leszczynski[30] using the TDDFT (B3-LYP) method agree well with our DFT/MRCI values at the equilibrium geometry optimized with the B3-LYP functional. As already noted, these values are somewhat lower than the corresponding ones at the BH-LYP geometry.

The dipole moment of the keto tautomer calculated at the LDA-DFT level[31] amounts to 6.71 D. Kwiatkowski and Leszczyński[32] obtained similar results with the HF method (7.12 D) and the DFT (B3-LYP) method (6.29 D). In photodetachment-photoelectron spectroscopy,[33] the dipole moment of the keto tautomer was predicted to be approximately 7 D, in good agreement with our DFT/MRCI value of 6.82 D.

There is also a number of experimental spectra reported for cytosine. In solution of trimethyl phosphate Clark and Tinoco[2] observed an absorption band at approximately 277 nm (4.5 eV). Absorption measurements in aqueous solution by Voelter et al.[3] reveal an absorption band with a maximum at 266 nm (4.66 eV). These bands can be assigned to a $\pi \rightarrow \pi^*$ transition in

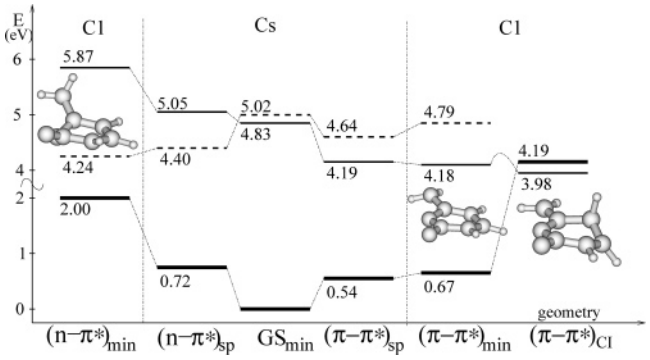

Figure 3. Spectrum of the keto cytosine (DFT/MRCI energies) at selected nuclear geometries. The nuclear arrangement was optimized at the BH-LYP level using C_s symmetry constraints and without any constraints. Minimum geometries are labeled by a subscript min, saddle-points by sp. The label CI denotes a point close to the conical intersection. The conical intersection occurs between the excited singlet $\pi \rightarrow \pi^*$ state and the electronic ground state. Solid lines: $^1\pi\pi^*$ state. Dashed lines: $^1n\pi^*$ state.

keto cytosine. They show agreement with the DFT/MRCI excitation energy of the lowest $^1\pi\pi^*$ state. A magnetic circular dichroism (MCD) spectrum of cytosine, measured by Voelter et al., yields an absorption band at about 270 nm (4.6 eV). Clark et al.[34] measured the vapor spectra of cytosine and found a shoulder in the long wavelength region at about 290 nm (4.28 eV). This much lower value is somewhat uncertain because the cytosine decomposes during these measurements and gives many other unidentified bands.[34] During the course of the present quantum chemical investigation, EELS (electron energy loss spectroscopy) measurements were carried out on cytosine under gas-phase conditions.[35] In these experiments the vertical $S_1 \leftarrow S_0$ excitation came out at 4.65 ± 0.1 eV. The comparison with earlier solution spectra implies that the solvent shift is small for this transition.

3.1.2. The Adiabatic Spectrum and Conical Intersections. The experimental R2PI spectra of cytosine were recorded close to the band origin and can therefore not be compared directly with vertical absorption spectra. For that purpose, we need adiabatic spectra. The order and the energies of the singlet excited states of keto cytosine depend strongly on the nuclear geometry (Figure 3).

At first, we have performed the energy minimization of the two lowest excited singlet states with C_s symmetry constraints by means of TDDFT (BH-LYP). The adiabatic DFT/MRCI excitation energy for the $n_O \rightarrow \pi_L^*$ state at the resulting stationary point amounts to 4.40 eV compared to a vertical absorption energy of 5.02 eV. In this region of the coordinate space the $^1n\pi^*$ state corresponds to the lowest-lying excited singlet (S_1). When the singlet excited $\pi_H \rightarrow \pi_L^*$ state is optimized under C_s symmetry constraints, its energy decreases from 4.83 eV at the ground-state geometry to 4.19 eV. The order of electronic states is similar to that in the vertical absorption region. However, the planar structures of the $^1\pi\pi^*$ and the $^1n\pi^*$ states correspond only to saddle points on the potential energy surface of these states.

Geometry optimization of the $n_O \rightarrow \pi_L^*$ state without symmetry constraints results in a strongly distorted excited-state structure (Figure 3, left side). The geometry change involves a pyramidalization of the amino group and significant out-of-plane deformations of the ring. The energy of this state is decreased from 4.40 eV in the C_s symmetric structure to 4.24 eV at the minimum.

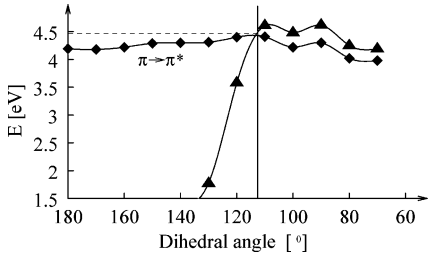

Figure 4. DFT/MRCI energies of the keto tautomer calculated along the TDDFT reaction path connecting the singlet $\pi \rightarrow \pi^*$ minimum and the conical intersection between the $^1\pi\pi^*$ state and the electronic ground state. The dihedral angle is the $N_1C_6C_5H$ angle. Below a value of 110° a constrained optimization of the excited state leads to a conical intersection at the TDDFT level. The TDDFT CMEP changes direction at the conical intersection. Triangles: electronic ground state. Diamonds: $\pi \rightarrow \pi^*$ state.

Unconstrained geometry optimization of the first excited $^1\pi\pi^*$ state results in an out-of-plane structure (Figure 3, right side). The nonplanarity is not only due to the pyramidalization of the amino group, but also the ring of cytosine is out-of-plane deformed and possesses a butterfly conformation. The adiabatic excitation energy of the $\pi \rightarrow \pi^*$ state amounts to 4.18 eV. C_s and C_1 energies of the singlet $\pi \rightarrow \pi^*$ state are very similar while the geometries differ strongly. The excited-state potential energy surface in that region is very flat. For a strict comparison with the experiment, ZPVE corrections have to be included. With these corrections, the $^1\pi\pi^*$ adiabatic excitation energy becomes 4.06 eV. The band origin of the experimental R2PI spectrum of the keto tautomer appears at around 32 000 cm^{-1} (3.97 eV). Taking into account the usual error-bars of the DFT/MRCI method, the spectral region of the keto form is predicted in good accord with experimental observations.

Motivated by the results of a recent quantum chemical study on the guanine−cytosine (GC) base pair[11] where a strongly deformed nuclear structure of the cytosine ring was obtained in the locally excited state, we studied the potential energy surface of the singlet $\pi_H \rightarrow \pi_L^*$ state for large out-of-plane distortions. The deformation involved a twisting of the $C_5{=}C_6$ double bond. This kind of out-of-plane distortion destabilizes the energy of the ground state which appears to be very sensitive to the twisting of the $C_5{=}C_6$ bond. Starting at a highly distorted geometry, the TDDFT gradient leads the system toward a conical intersection with the electronic ground state (Figure 3, right side). Beside the twisting of the $C_5{=}C_6$ bond, the deformation involves an elongation of this bond from 1.34 Å in the ground state to 1.44 Å in the excited $\pi \rightarrow \pi^*$ state. These results resemble the behavior of the excited singlet state in the GC base pair.[11]

To obtain an estimate of the barrier height between the minimum and conical intersection areas on the potential energy surface of the S_1 state we performed a constrained energy optimization at the TDDFT level. The proper internal coordinate for this purpose was found to be the dihedral angle $N_1-C_6-C_5-H$. We kept this angle fixed while relaxing all other internal degrees of freedom. Note that for dihedral angles of 110° and below, the geometry optimization breaks off when the electronic ground-state hits the intersection seam. These points might, therefore, not be located on the true TDDFT minimum energy path. After partial optimizations, single-point DFT/MRCI calculations were performed. The CMEP is presented in Figure 4. For dihedral angles between 170 and 120°, the first excited state corresponds to the $\pi_H \rightarrow \pi_L^*$ transition. For smaller values of the angle the order of the $^1\pi\pi^*$ state and the ground state is interchanged. The lowest point of the conical intersection seam

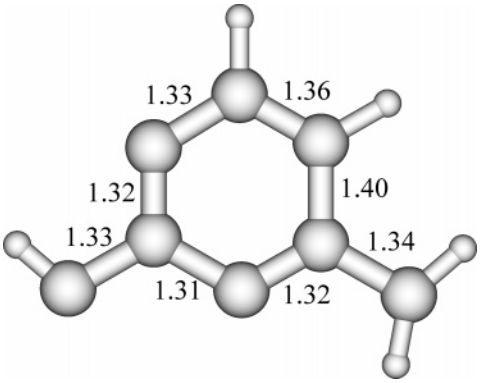

Figure 5. Ground-state geometry of the enol tautomer optimized with the BH-LYP functional. DFT/MRCI energy: $-394.849073E_H$. Dipole moment at the DFT/MRCI level: 3.55 D.

is reached at about 70° (3.98 eV). The energy difference between the minimum in the FC region and the highest point on the CMEP amounts to merely 0.2 eV. The presence of conical intersections between the $^1(\pi \rightarrow \pi^*)$ state and the electronic ground state that is separated from the $^1(\pi \rightarrow \pi^*)$ minimum in the FC region by a small barrier, explains the experimental finding that only a few sharp vibronic peaks close to the band origin could be observed in the R2PI spectrum of keto cytosine.[1,36] As soon as the conical intersection can be accessed—either directly or via a tunneling process—the excited state population is rapidly transferred to the electronic ground-state surface and the spectrum breaks off.

Merchán and Serrano-Andrés in their CASSCF/CASPT2 study[13] found another (gs/$\pi\pi^*$) conical intersection of the keto tautomer. According to these calculations, the crossing occurs along the C═O stretching mode at a bond distance of 1.428 Å and very little energy is needed to overcome a barrier (0.1 eV) and the excited-state surface rapidly decays to the ground-state surface. The conical intersection obtained in our study is not identical with the one described by Merchán and Serrano-Andrés. Its nuclear structure exhibits a C═O bond length of 1.19 Å, similar to the ground-state equilibrium distance. The conical intersection of the potential energy surfaces along the C_5═C_6 twisting coordinate rather represents an alternative pathway for the ultrafast decay of the excited state of the keto cytosine to its electronic ground state.

3.2. Enol Tautomer of Cytosine. Our investigation of the electronic ground state of the enol tautomer has shown that it is the most stable form in the gas phase. Among all the tautomers of cytosine, the enol form has the smallest dipole moment. Upon DFT (B3-LYP) optimization without symmetry constraints, the geometry exhibits deformations which include a slight pyramidalization of the amino group. However, the energy change with respect to the C_s-symmetric structure obtained at the same level of theory is negligible (0.001 eV). Employing the BH-LYP functional, a planar nuclear arrangement has been found for the ground state minimum. For further calculations of vertical and adiabatic absorption spectra we have used the BH-LYP equilibrium structure of the ground state geometry which is presented in Figure 5. Utilizing the SNF program we have calculated the harmonic vibrational frequencies for the ground state (Table 3). The scaled frequencies show good agreement with the experimentally observed ones, displayed alongside in Table 3.

3.2.1. The Vertical Absorption Spectrum. We begin the description of the excited-state electronic structure with the characterization of the molecular orbitals. The highest occupied molecular orbital (HOMO) is a π-type orbital, designated by π_H. It belongs to the a″ irreducible representation and is

TABLE 3: Harmonic Vibrational Frequencies [cm^{-1}] for the NH Stretching Modes in the Ground State of the Enol Cytosine[a]

	DFT(B3-LYP, scaled)	experiment[25]	experiment[26]
NH_2(s)	3459	3450	3456
NH_2(a)	3583	3575	3572
OH	3620	3620	3610

[a] Key: (s) symmetric vibrations; (a) antisymmetric vibrations.

TABLE 4: Vertical Singlet Excitation Energies ΔE [eV] (DFT/MRCI, TZVP Basis, BH-LYP Geometry) and Dipole Transition Oscillator Strengths $f(r)$ of Enol Cytosine

		DFT/MRCI, present work		
state		ΔE	$f(r)$	dominant excitation(s)
S_1	$2^1A'$	5.14	0.1389	$\pi_H \rightarrow \pi^*_L$
S_2	$1^1A''$	5.27	0.0096	$n_N \rightarrow \pi^*_L$
S_3	$2^1A''$	5.99	0.0008	$n_N \rightarrow \pi^*_{L+1}$
S_4	$3^1A'$	6.13	0.1515	$\pi_H \rightarrow \pi^*_{L+1}$, $\pi_{H-1} \rightarrow \pi^*_L$
S_5	$3^1A''$	6.35	0.0013	$(\pi_H \rightarrow \text{Ryd})^a$
S_6	$4^1A'$	6.68	0.2088	$\pi_{H-1} \rightarrow \pi^*_L$, $\pi_H \rightarrow \pi^*_{L+1}$
S_7	$4^1A''$	6.84	0.0003	$n_O \rightarrow \pi^*_L$

[a] When diffuse functions are added to the basis, the energy of the Rydberg excitation is expected to decrease considerably.

delocalized over the whole molecule. The second highest occupied molecular orbital (HOMO-1) is an n-type orbital. It exhibits large amplitudes for the N_1, N_3, and N_8 lone-pair orbitals and we designate it as n_N. The third highest occupied molecular orbital (HOMO-2) is of π-type, denoted by π_{H-2}. The fourth highest occupied molecular orbital (n_O) is a nonbonding (n-type) orbital with large amplitudes for the oxygen, N_1, and N_3 lone-pair orbitals. We begin the characterization of the virtual orbitals with the lowest-lying unoccupied molecular orbital (LUMO). This is a π-type orbital which we denote by π^*_L. The next higher valence orbital is π^*_{L+1}. Both orbitals belong to the a″ irreducible representation.

The DFT/MRCI excitation energies, oscillator strengths, and dominant excitations have been computed at the BH-LYP geometry and are presented in Table 4. The first singlet excited state is a $\pi \rightarrow \pi^*$ state, and it corresponds to the HOMO−LUMO transition. It appears to be very strong. The second excited singlet state $1^1A''$ arises from an excitation out of the highest occupied nonbonding orbital (n_N) to the π^*_L. This transition has a small oscillator strength. The third excited singlet state S_3 results from an excitation out of the n_N orbital to π^*_{L+1}. The oscillator strength for this transition is found to be very small. The fourth excited singlet state S_4 is again a $\pi \rightarrow \pi^*$ state. The MRCI expansion of this state is mixed and contains two dominant excitations: $\pi_H \rightarrow \pi^*_{L+1}$ and $\pi_{H-1} \rightarrow \pi^*_L$. It appears as a very strong transition.

When we compare the vertical spectra at different geometries we notice that the spectrum at the B3-LYP geometry is slightly shifted to lower energies. The first excited $\pi \rightarrow \pi^*$ state at the BH-LYP geometry has an energy of 5.14 eV while at the B3-LYP geometry its energy is 5.02 eV. The lowest $n \rightarrow \pi^*$ state exhibits the same behavior. Its energy changes from 5.27 eV at the BH-LYP geometry to 5.20 eV at the B3-LYP geometry. However, the ordering of the excited states remains the same.

The stability of the enol tautomer and its dipole moment in the ground-state agree very well with the results of previous theoretical studies.[37,38] The RI-MP2 calculations for the gas phase by Hobza et al.[38] predict that the enol is the most stable form of cytosine. They obtain a dipole moment in the ground state of 3.25 D. Yang and Rodgers[37] calculated the dipole

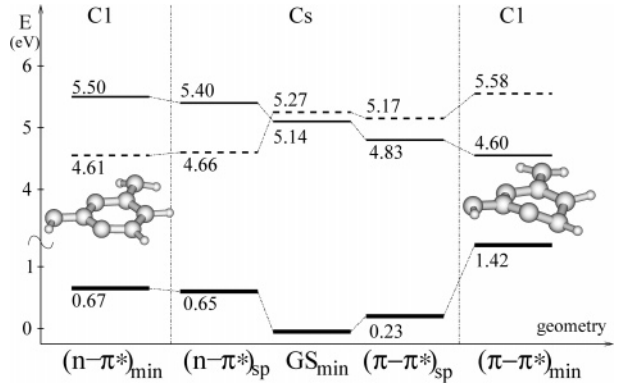

Figure 6. Spectrum of the enol cytosine (DFT/MRCI energies) at selected nuclear geometries. The sketched distorted geometry on the right side corresponds to the minimum of the first excited $\pi \rightarrow \pi^*$ state and on the left side to the minimum of the first $n \rightarrow \pi^*$ excited state. Solid lines: $^1\pi\pi^*$ state. Dashed lines: $^1n\pi^*$ state. See Figure 3 for further explanations.

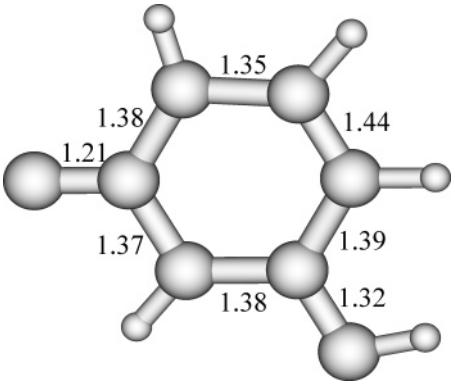

Figure 7. Ground-state geometry of the keto−imine tautomer optimized with the BH-LYP functional. DFT/MRCI energy: −394.847069 E_H. Dipole moment at the DFT/MRCI level: 4.92 D.

moment of the enol form to be 3.72 D at the MP2(full)/6-31G* level. The LDA-DFT method[31] predicted a value of 3.51 D. Kwiatkowski and Leszczyński[32] using the HF and DFT (B3-LYP) approaches calculated the dipole moment to be 3.39 and 3.16 D, respectively. The experimental finding from the photodetachment-photoelectron spectroscopy[33] amounts to 3.4 D. Our DFT/MRCI value of 3.55 D is in accordance with these results.

The vertical absorption spectrum for enol cytosine was predicted by the semiempirical INDO/s method.[39] The $\pi \rightarrow \pi^*$ transition energies are underestimated and differ from our DFT/MRCI values. According to the INDO/s approach, the lowest-lying $\pi \rightarrow \pi^*$ state appears at 37 100 cm^{-1} (4.59 eV) while we find an excitation energy of 5.14 eV at the BH-LYP geometry. The authors also suggested that the lowest-lying $n \rightarrow \pi^*$ state is the third excited state with an energy of 46 800 cm^{-1} (5.80 eV). In the DFT/MRCI, the $n \rightarrow \pi^*$ state appears as the second transition with an energy of 5.27 eV.

3.2.2. The Adiabatic Spectrum and Excited-State Geometry. The adiabatic excitation energy represents the energy difference between the ground state equilibrium and the optimized excited-state structure. When ZPVE corrections are taken into account, this energy is roughly comparable to the 0−0 transition in the experimental R2PI spectrum. By means of TDDFT, we have first optimized excited states under C_s-symmetry constraints (Figure 6). The DFT/MRCI excitation energy of the $n \rightarrow \pi^*$ state decreases from 5.27 eV at the ground-state minimum to 4.66 eV at the optimized planar structure. Here, the $n \rightarrow \pi^*$ state becomes the lowest-lying excited state. The minimal excitation energy of the planar $\pi \rightarrow \pi^*$ state is 4.83 eV. The optimization stabilizes this state by about 0.3 eV with respect to its energy at the ground-state geometry (5.14 eV).

Unconstrained geometry optimization of the lowest $n \rightarrow \pi^*$ state leads to an out-of-plane distorted minimum structure (Figure 6, left side). The deformation refers to the pyramidalization of the NH_2 group while the ring geometry remains planar. Because of the small geometry change, the adiabatic excitation energy of the $n \rightarrow \pi^*$ state (4.61 eV) is only slightly decreased with respect to the excitation energy of the C_s symmetric structure (4.66 eV).

The optimized C_s symmetric structure of the $^1\pi\pi^*$ state represents only a saddle point on the potential energy surface. Unconstrained geometry optimization of this state leads to an out-of-plane distorted structure (Figure 6, right side). Comparison of the C_s- and C_1-symmetric structures shows that the geometry change upon electronic excitation involves not only a pyramidalization of the amino group, but also deformation of the ring itself. The adiabatic excitation energy of the distorted $^1\pi\pi^*$ state of enol cytosine amounts to 4.60 eV, corresponding to a stabilization by more than 0.5 eV with respect to its value at the ground-state minimum. Taking into account the scaled ZPVE of the ground and excited state, the adiabatic excitation energy of the $^1\pi\pi^*$ state of the enol tautomer becomes 4.50 eV. The origin of the experimental R2PI spectrum was observed around 36 000 cm^{-1} (4.46 eV). Comparing these results, we conclude that the DFT/MRCI approach predicts the spectral region of enol cytosine in good agreement with experiment. The geometric relaxation on the $^1\pi\pi^*$ potential energy surface involves a twisting of the C_5═C_6 double bond and also its elongation from 1.36 Å in the ground state to 1.44 Å at the singlet $\pi\pi^*$ minimum. The energy of the ground state at this nonplanar geometry is significantly increased and shows a strong dependence on the out-of-plane deformations. However, no conical intersection was encountered during the optimization. We therefore expect that low-lying vibrational levels in the $^1\pi\pi^*$ state of the enol form of cytosine decay by normal internal conversion, possibly through coupling to nearby $^1n\pi^*$ levels. This process is slow compared to a decay via a conical intersection and should allow the observation of many sharp spectral lines, in accord with experimental findings.

3.3. Keto—Imine Tautomer of Cytosine. The third structural isomer of cytosine that we investigate is known as the keto−imine tautomer. Energetically, this is the least stable form in the gas phase among the three tautomers. The dipole moment of the keto−imine lies between the values for the keto and the enol tautomers. The ground-state optimization was performed with and without C_s symmetry constraints. In the latter case, the structure converged to the planar form and the energy remained the same as for the C_s-symmetric structure. The keto−imine does not possess the NH_2 group and thus exhibits no pyramidalization effect. The equilibrium ground-state geometry, the dipole moment, and the DFT/MRCI energy of the keto−imine are shown in Figure 7.

Employing the SNF program, we have calculated the harmonic vibrational frequencies in the ground state of this tautomer. The scaled frequencies are presented in Table 5. As experimental values are not available, these data can be used as a lead to identify this tautomer in forthcoming IR−UV double-resonance experiments.

3.3.1. The Vertical Absorption Spectrum. For the description of the electronic structure of the excited states, it is necessary at first to assign the orbital nature. The highest

TABLE 5: Harmonic Vibrational Frequencies [cm^{-1}] for the NH Stretching Modes in the Ground State of the Keto−Imine Cytosine

	DFT(B3-LYP, scaled)
N_8H	3370
N_3H	3458
N_1H	3500

TABLE 6: Vertical Singlet Excitation Energies ΔE [eV] (DFT/MRCI, TZVP Basis, BH-LYP Geometry) and Dipole Transition Oscillator Strengths $f(r)$ of Keto−Imine Cytosine

		DFT/MRCI, present work		
state		ΔE	$f(r)$	dominant excitation(s)
S_1	$1^1A''$	5.19	0.0055	$n_N \rightarrow \pi^*_L$
S_2	$2^1A'$	5.26	0.2949	$\pi_H \rightarrow \pi^*_L$
S_3	$3^1A'$	5.96	0.0210	$\pi_{H-1} \rightarrow \pi^*_L$
S_4	$2^1A''$	6.18	0.0001	$n_O \rightarrow \pi^*_L$, $n_O \rightarrow \pi^*_{L+1}$
S_5	$3^1A''$	6.32	0.0003	$(\pi_H \rightarrow \mathrm{Ryd})^a$
S_6	$4^1A'$	6.55	0.3537	$\pi_H \rightarrow \pi^*_{L+1}$
S_7	$4^1A''$	7.04	0.0007	$n_N \rightarrow \pi^*_{L+1}$, $n_O \rightarrow \pi^*_L$

[a] When diffuse functions are added to the basis, the energy of the Rydberg excitations is expected to decrease considerably.

occupied molecular orbital (HOMO) is a π-type orbital, designated by π_H. The second highest occupied molecular orbital (HOMO-1) belongs also to the π-type orbitals and we denote it by π_{H-1}. The third highest occupied molecular orbital is a nonbonding orbital with a large amplitude for the N_3 lone-pair orbital. We designate it by n_N. The fourth highest occupied molecular orbital (HOMO-3) is an n-type orbital with large amplitude for the carbonyl oxygen, N_1, and N_3 lone-pair orbitals and is labeled by n_O. We begin the assignment of the virtual orbitals with the lowest unoccupied molecular orbital (LUMO). This is a π-type orbital designated by π^*_L. In the energy gap between the LUMO and the next valence molecular orbital we find one diffuse orbital. Nevertheless, the higher valence orbitals will be denominated π^*_{L+1}, π^*_{L+2}, etc.

Vertical excitation energies of the keto−imine, oscillator strengths, and dominant excitations are given in Table 6. The lowest-lying singlet state does not correspond to a HOMO−LUMO transition. It results from an excitation out of the highest occupied nonbonding molecular orbital (n_N) to the π^*_L orbital. As is expected for $n \rightarrow \pi^*$ transitions, its oscillator strength is small. The second excited singlet state S_2 arises from the HOMO−LUMO transition. This transition is found to be very strong. The third excited singlet state is also a $\pi \rightarrow \pi^*$ state. The transition is accompanied by a charge transfer from the oxygen into the ring. Its oscillator strength is small. The fourth excited-state S_4 originates from two dominant excitations: one corresponds to the promotion of an electron out of the n_O orbital to the π^*_L, and the other to the promotion of an electron from the n_O to the π^*_{L+1} orbital. The oscillator strength for this transition is found to be very small.

Comparing the vertical spectra at the BH-LYP and the B3-LYP geometries, we confirm our expectations that the B3-LYP geometry exhibits longer bond distances and yields lower excitation energies. The vertical excitation energy of the lowest $n \rightarrow \pi^*$ state changes from 5.19 eV at the BH-LYP geometry to 5.10 eV at the B3-LYP geometry. The energy of the first excited $\pi \rightarrow \pi^*$ state is lowered from 5.26 eV at the BH-LYP to 5.12 eV at the B3-LYP geometry.

Here we make a comparison of our results with the previous theoretical treatments of the keto−imine tautomer. The relative stability of isolated cytosine tautomers in the gas phase, including the imino form, has been examined by Hobza et al.[38] They performed ground-state optimizations at the RIMP2/TZVPP level of theory and found that the keto−imine form is the least stable in the gas phase with a dipole moment of 4.63 D. The DFT/MRCI value amounts to 4.92 D. In agreement with our results, Hobza et al.[38] find that the keto−imine form is planar in the ground state whereas the keto and enol forms exhibit a pyramidalization of the amino groups. Employing the HF and DFT (B3-LYP) methods,[32] its dipole moment is found to be 5.19 and 4.57 D, respectively. The relative stabilities of the cytosine tautomers determined at the MP2(full)/6−31 G^* level of theory by Yang and Rodgers[37] agree well with our results, whereas the dipole moment of the keto−imine tautomer (5.46 D) is somewhat larger than the one we obtain with the DFT/MRCI method. The calculated value in the LDA-DFT approach[31] (4.83 D) is in a good agreement with our finding. Investigations by Shukla and Leszczynski[30] employing the TDDFT (B3-LYP) method, confirm the order of stability in the gas phase for cytosine tautomers. Their computed dipole moment of the keto−imine form (5.12 D) is in very good agreement with the DFT/MRCI result.

Shukla and Leszczynski[30] also calculated vertical $\pi\pi^*$ and $n\pi^*$ excitation energies. In the TDDFT study the lowest-lying $\pi \rightarrow \pi^*$ state appears at 4.77 eV. This value is lower than the one we find in the DFT/MRCI at the BH-LYP geometry (5.26 eV). The second excited $^1\pi\pi^*$ state is computed to appear at 5.97 eV. This value agrees very well with the one we obtain for the second $\pi \rightarrow \pi^*$ transition (5.96 eV). The lowest $n \rightarrow \pi^*$ state in the TDDFT method has the energy of 5.13 eV. This value agrees with our excitation energy for the first excited $^1n\pi^*$ state (5.19 eV). Because the absorption spectrum of the keto−imine form could not be measured yet, a comparison of the vertical excitation energies with experiment is not possible.

3.3.2. The Adiabatic Spectrum and Excited-State Geometry. We have optimized the geometries of the singlet excited $n \rightarrow \pi^*$ and $\pi \rightarrow \pi^*$ states. In the beginning we restrict the symmetry to C_s. The minimal excitation energy (confined to a planar structure) for the $n \rightarrow \pi^*$ transition is 4.22 eV, compared to a vertical absorption energy of 5.19 eV. The optimized structure of the $^1\pi\pi^*$ state has an energy of 4.50 eV which is considerably decreased with respect to its value at the ground-state minimum (5.26 eV).

As for the other tautomers, we wanted to investigate possible out-of-plane structures of the excited states. Therefore, we performed unconstrained geometry optimizations. At small deviations from planarity the first excited state is the $n \rightarrow \pi^*$ state. Optimizing the energy of this state, we obtain a structure which contains a planar ring with a pronounced out-of-plane deviation of the NH group (Figure 8, left side). The C_4N_8H angle is 108° with the NH group almost perpendicular to the ring itself. The adiabatic excitation energy of the $^1n\pi^*$ state amounts to merely 3.32 eV. Including the scaled ZPVE corrections, it is decreased to 3.27 eV. This is the lowest-lying excited state of the keto−imine tautomer. Its energy is much lower than the one for the planar structure, confirming that the C_s symmetric structure represents only a saddle point on the potential energy surface of this state. The large difference between the vertical and adiabatic excitation energies implies that the Franck−Condon factor for the 0−0 transition will be very small.

The unconstrained geometry optimization of the singlet $\pi \rightarrow \pi^*$ state stabilizes the energy of this state, but destabilizes strongly the energy of the ground state. To find the minimum of this state we have employed a normal-mode analysis. Small distortions were made along the normal mode with the negative

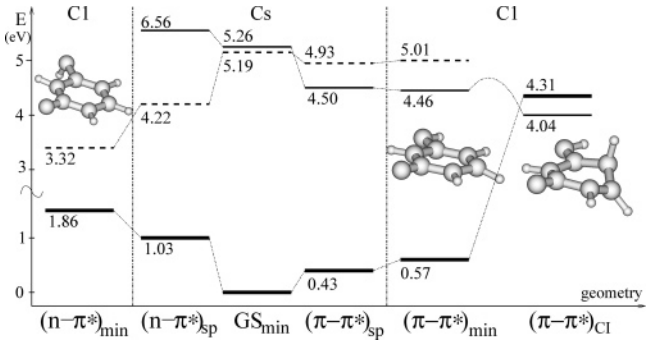

Figure 8. Spectrum of the keto−imine cytosine (DFT/MRCI energies) at selected nuclear geometries. The sketched geometry on the left side corresponds to the minimum of the first excited n → π^* state. The structure of the conical intersection which occurs between the singlet $\pi \rightarrow \pi^*$ excited state and the electronic ground state is shown on the right side. Solid lines: $^1\pi\pi^*$ state. Dashed lines: $^1n\pi^*$ state. See Figure 3 for further explanations.

frequency and the DFT/MRCI energies were calculated at these points. The minimum structure of the $\pi \rightarrow \pi^*$ state is almost planar, with slight out-of-plane deviations. Its energy amounts to 4.46 eV and the potential energy surface in the region between the planar stationary point and the minimum is very flat. The ground state appears to be very sensitive to the out-of-plane distortions. The excited-state gradient leads the system toward a conical intersection with the electronic ground state. Energetically, the crossing occurs at about 4 eV. The distortion involves a twisting of the C_5═C_6 bond accompanied by an elongation from 1.35 Å at the ground-state equilibrium to 1.45 Å in the excited $\pi \rightarrow \pi^*$ state. The out-of-plane deformation and the observed crossing in the $^1\pi\pi^*$ state resemble the behavior of the first excited $\pi \rightarrow \pi^*$ state of the keto tautomer of cytosine. The adiabatic spectrum of the keto−imine including the distorted excited-state structures is presented in Figure 8.

After detection of a crossing between the $^1\pi\pi^*$ state and the ground state, a question about the reaction energy path and barrier height arose. For that purpose constrained energy optimizations on the S_1 potential energy surface were performed. An appropriate reaction coordinate was found to be the dihedral angle $N_1-C_6-C_5-H$. After having accomplished the partial TDDFT optimizations, single-point DFT/MRCI calculations were carried out. Note that the geometry optimization breaks off when the electronic ground state hits the seam of conical intersections. The points obtained for dihedral angles below 130°, might therefore, not be located on the true TDDFT minimum energy path. The calculated reaction path is presented in Figure 9. For dihedral angles smaller than 130°, the system runs into a conical intersection. The lowest point on the intersection seam is reached at approximately 70° (4.04 eV). When the chosen dihedral angle is between 130° and 160°, the first excited state corresponds to a $\pi_H \rightarrow \pi_L^*$ excitation. For the geometries close to the planar one, the order of the $^1\pi\pi^*$ and $^1n\pi^*$ states is interchanged. The n → π^* minimum is located well below the conical intersection between the S_1 and S_0 states. At more distorted geometries, the higher-lying singlet $\pi \rightarrow \pi^*$ state can decay to the ground state via an almost barrierless reaction path.

In high-resolution R2PI measurements this cytosine tautomer has not been observed so far, although its population is estimated to be about one-quarter of the population of the keto and enol tautomers.[10] On the basis of our theoretical results, we attribute the lack of its observation to the following reasons. The lowest-lying excited singlet state of the keto−imine is the n → π^* state. The DFT/MRCI calculations have shown that its adiabatic

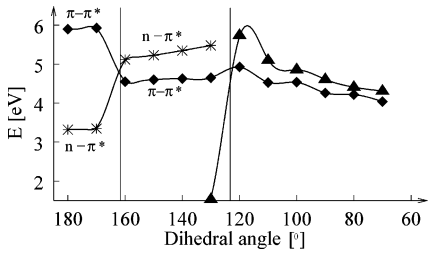

Figure 9. DFT/MRCI energies of the keto−imine tautomer calculated along the TDDFT reaction path connecting the singlet n → π^* minimum and the conical intersection between the $^1\pi\pi^*$ state and the electronic ground state. The dihedral angle is the $N_1C_6C_5H$ angle. Below a value of 130° a constrained optimization of the excited state leads to a conical intersection at the TDDFT level. The TDDFT CMEP changes directions at the conical intersections. Triangles: electronic ground state. Diamonds: $\pi \rightarrow \pi^*$ state. Stars: n → π^* state.

excitation energy lies in the low-frequency spectral region corresponding to a laser wavelength of 373 nm. This spectral region has not been scanned by Nir et al.[7] In addition to the small electronic dipole transition moment, the FC-factors are small due to the large geometry shift. The first excited $^1(\pi \rightarrow \pi^*)$ state undergoes conical intersections with the ^{1}(n → π^*) state and the electronic ground state which cause its very short lifetime and possibly disable it to be observed in the experimental spectrum. It remains to be seen whether the experiment will confirm these findings.

4. Summary and Conclusions

In the present work the keto, enol, and keto−imine tautomers of cytosine have been investigated by combined density functional and multireference configuration interaction methods. It is found that the enol form is the most stable tautomeric form in the gas phase. The order of stability for the tautomers according to our findings is as follows: keto−imine < keto < enol. Nevertheless, due to its larger dipole moment, the keto tautomer may be preferentially stabilized in aqueous environments and in other polar solvents.

Our main aim was to study the excited states of the above-mentioned cytosine tautomers and to explain their experimentally observed high-resolution resonant two-photon ionization (R2PI) vibronic spectra. For the comparison with these spectra the computed adiabatic excitation energies were used. As a response to electronic excitation, significant changes in geometry take place. Upon relaxation, a loss of planarity occurs for the lowest-lying singlet $\pi \rightarrow \pi^*$ and n → π^* states of all three tautomers investigated.

For the keto tautomer, the form in which cytosine appears in DNA, a distorted butterfly conformation of the $^1\pi\pi^*$ state is found. Its adiabatic excitation energy computed at the DFT/MRCI level (4.06 eV including ZPVE corrections) supports the assignment of the R2PI bands around 32 000 cm^{-1} (∼4 eV) to the keto tautomer. We have explored an energy reaction path for twisting the C_5═C_6 double bond in the cytosine ring. A conical intersection between the lowest excited $\pi \rightarrow \pi^*$ state and the ground state has been located on this path. After excitation of the S_1 state, the conical intersection becomes accessible via a reaction with a small energy barrier above the origin, thus enabling rapid internal conversion to the electronic ground state.

For the $^1\pi\pi^*$ state of the enol tautomer we have obtained a minimum at a distorted nuclear arrangement which involves a twisting and an elongation of the C_5═C_6 bond. It is located at considerably higher excitation energies (4.50 eV including ZPVE corrections) than the corresponding transition in the keto

form, in excellent accord with the experimental observation of bands around 36 000 cm^{-1} (~4.5 eV). From the large difference between the ground and excited-state geometries, long vibrational progressions are expected to occur in the vibronic spectrum. A conical intersection has not been located close to the minimum in this case. On these grounds, the low-lying vibronic bands of the $^1(\pi \rightarrow \pi^*)$ transition are predicted to be long-lived compared to those of the keto form.

The examination of the excited states of the keto−imine tautomer has shown that the lowest-lying excited singlet state is the $n \rightarrow \pi^*$ state. The torsion of the imine group with respect to the ring plane leads to an extremly low excitation energy (3.27 eV). The oscillator strength for this transition is very small. In addition, for this tautomer a conical intersection between the $\pi \rightarrow \pi^*$ excited state and the electronic ground state has been identified that can be reached from the Franck−Condon area without passing over a barrier. The $^1\pi\pi^*$ minimum in this case is located close to planarity at the energy of 4.46 eV and spontaneously decays to the ground state. The experimental detection of the electronic excitation spectrum of this tautomer thus remains a challenge for future spectroscopic investigations.

The present work reveals that the cytosine tautomers exhibit significant structural changes upon electronic excitations. Our quantum chemical calculations, based on combined density functional/multireference configuration interaction method, were able to provide many valuable information about the energies and geometries of the nonplanar excited states of cytosine.

Acknowledgment. It is a pleasure to thank Profs. Karl Kleinermanns and Rainer Weinkauf from the Physical Chemistry Department of the Heinrich Heine University Düsseldorf for many valuable discussions.

Supporting Information Available: Tables of Cartesian coordinates of ground and excited-state minima of all tautomers and the coordinates of nuclear structures at (or close to) conical intersections between the ground state and the first excited singlet $\pi \rightarrow \pi^*$ states of the keto and the keto−imine tautomers. This material is available free of charge via the Internet at http://pubs.acs.org.

References and Notes

(1) Crespo-Hernandez, C. E.; Cohen, B.; Hare, P. M.; Kohler, B. *Chem. Rev.* **2004**, *104*, 1977−2019.

(2) Clark, L. B.; Tinoco, I., Jr. *J. Am. Chem. Soc.* **1965**, *87*, 11−15.

(3) Voelter, W.; Records, R.; Bunnenberg, E.; Djerassi, C. *J. Am. Chem. Soc.* **1968**, *90*, 6163−6170.

(4) Pecourt, J.-M. L.; Peon, J.; Kohler, B. *J. Am. Chem. Soc.* **2000**, *122*, 9348−9349.

(5) Pecourt, J.-M. L.; Peon, J.; Kohler, B. *J. Am. Chem. Soc.* **2001**, *123*, 10370−10378.

(6) Peon, J.; Zewail, A. H. *Chem. Phys. Lett.* **2001**, *348*, 255−262.

(7) Nir, E.; Hünig, I.; Kleinermannns, K.; de Vries, M. S. *Phys. Chem. Chem. Phys.* **2003**, *5*, 4780−4785.

(8) Nir, E.; Müller, M.; Grace, L. I.; de Vries, M. S. *Chem. Phys. Lett.* **2002**, *355*, 59−64.

(9) Canuel, C.; Mons, M.; Piuzzi, F.; Tardivel, B.; Dimicoli, I.; Elhanine, M. *J. Chem. Phys.* **2005**, *122*, 074316.

(10) Brown, R. D.; Godfrey, P. D.; McNaughton, D.; Pierlot, A. P. *J. Am. Chem. Soc.* **1989**, *111*, 2308−2310.

(11) Sobolewski, A. L.; Domcke, W. *Phys. Chem. Chem. Phys.* **2004**, *6*, 2763−2771.

(12) Abo-Riziq, A.; Grace, L.; Nir, E.; Kabelac, M.; Hobza, P.; de Vries, M. *PNAS* **2005**, *102*, 20−23.

(13) Merchán, M.; Serrano-Andrés, L. *J. Am. Chem. Soc.* **2003**, *125*, 8108.

(14) Schäfer, A.; Huber, C.; Ahlrichs, R. *J. Chem. Phys.* **1994**, *100*, 5829.

(15) Marian, C. M. *J. Chem. Phys.* **2005**, *122*, 104314.

(16) Turbomole (vers. 5.6). Ahlrichs, R.; Bär, M.; Baron, H.-P.; Bauernschmitt, R.; Böcker, S.; Deglmann, P.; Ehrig, M.; Eichkorn, K.; Elliott, S.; Furche, F.; Haase, F.; Häser, M.; Hättig, C.; Horn, H.; Huber, C.; Huniar, U.; Kattannek, M.; Köhn, A.; Kölmel, C.; Kollwitz, M.; May, K.; Ochsenfeld, C.; Öhm, H.; Schäfer, A.; Schneider, U.; Sierka, M.; Treutler, O.; Unterreiner, B.; von Arnim, M.; Weigend, F.; Weis, P.; Weiss, H. Universität Karlsruhe, 2002.

(17) Furche, F.; Ahlrichs, R. *J. Chem. Phys.* **2002**, *117*, 7433−7447.

(18) Becke, A. D. *J. Chem. Phys.* **1993**, *98*, 5648−5652.

(19) Lee, C.; Yang, W.; Parr, R. G. *Phys. Rev. B* **1988**, *37*, 785.

(20) ef.x program for optimization by eigenvector following. Grimme, S. Universität Bonn, 1994.

(21) Snf (v. 2.2.1.). Kind, C.; Reiher, M.; Neugebauer, J.; Hess, B. A. Universität Erlangen, 1999.

(22) Koch, W.; Holthausen, M. C. *A Chemist's Guide to Density Functional Theory*. Wiley−VCH Verlag: Weinheim, Germany, 2001.

(23) Grimme, S.; Waletzke, M. *J. Chem. Phys.* **1999**, *111*, 5645.

(24) Zhou, X.; Wheeless, C. J. M.; Liu, R. *Vibr. Spectrosc.* **1996**, *12*, 53−63.

(25) Nir, E.; Plützer, C.; Kleinermanns, K.; de Vries, M. *Eur. Phys. J. D* **2002**, *20*, 317−329.

(26) Dong, F.; Miller, R. E. *Science* **2002**, *298*, 1227−1230.

(27) Petke, J. D.; Maggiora, G. M.; Christoffersen, R. E. *J. Phys. Chem.* **1992**, *96*, 6992−7001.

(28) Fülscher, M. P.; Roos, B. O. *J. Am. Chem. Soc.* **1995**, *117*, 2089−2095.

(29) Ismail, N.; Blancafort, L.; Olivucci, M.; Kohler, B.; Robb, M. A. *J. Am. Chem. Soc.* **2002**, *124*, 6818.

(30) Shukla, M. K.; Leszczynski, J. *J. Phys. Chem. A* **2002**, *106*, 11338−11346.

(31) Astrin, D. A.; Paglieri, L.; Corongiu, G. *J. Phys. Chem.* **1994**, *98*, 5653−5660.

(32) Kwiatkowski, J. S.; Leszczyński, J. *J. Phys. Chem.* **1996**, *100*, 941−953.

(33) Schiedt, J.; Weinkauf, R.; Neumark, D. M.; Schlag, E. W. *J. Chem. Phys.* **1998**, *239*, 511−524.

(34) Clark, L. B.; Peschel, G. G.; Tinoco, I., Jr. *J. Phys. Chem.* **1965**, *69*, 3615−3618.

(35) Abouaf, R.; Pommier, J.; Dunet, H.; Quan, P.; Nam, P.; Nguyen, M. T. *J. Chem. Phys.* **2004**, *121*, 11668−11674.

(36) Malone, R. J.; Miller, A. M.; Kohler, B. *Photochem. Photobiol.* **2003**, *77*, 158−164.

(37) Yang, Z.; Rodgers, M. T. *Phys. Chem. Chem. Phys.* **2004**, *6*, 2749−2757.

(38) Trygubenko, S. A.; Bogdan, T. V.; Rueda, M.; Orozco, M.; Luque, F. J.; Šponer, J.; Slav×c1ček, P.; Hobza, P. *Phys. Chem. Chem. Phys.* **2002**, *4*, 4192−4203.

(39) Broo, A.; Holmén, A. *J. Phys. Chem. A* **1997**, *101*, 3589−3600.